Fabrication of Supramolecular n/p-Nanowires *via* Coassembly of Oppositely Charged Peptide-Chromophore Systems in Aqueous Media

Mohammad Aref Khalily,[†] Gokhan Bakan,[†,‡] Betul Kucukoz,[§,‖] Ahmet Emin Topal,[†] Ahmet Karatay,[§] H. Gul Yaglioglu,[§] Aykutlu Dana,[†] and Mustafa O. Guler*[,†,⊥]

[†]Institute of Materials Science and Nanotechnology and National Nanotechnology Research Center (UNAM), Bilkent University, Ankara 06800, Turkey
[‡]Department of Electrical and Electronics Engineering, Atilim University, Ankara 06836, Turkey
[§]Department of Physics Engineering, Ankara University, Ankara 06100, Turkey
[‖]Department of Chemistry and Chemical Engineering, Chalmers University of Technology, 41296 Gothenburg, Sweden
[⊥]Institute for Molecular Engineering, University of Chicago, Chicago, Illinois 60637, United States

S *Supporting Information*
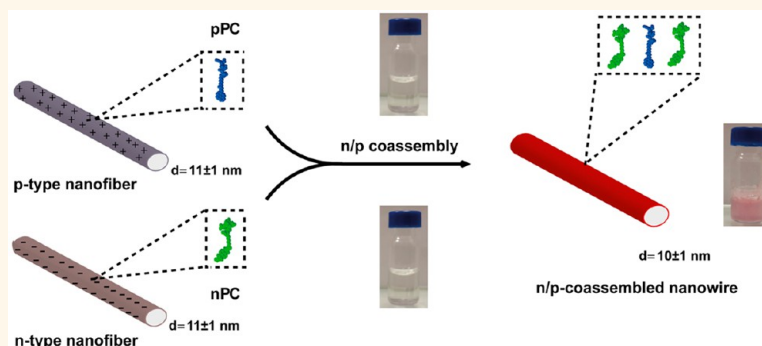
ABSTRACT: Fabrication of supramolecular electroactive materials at the nanoscale with well-defined size, shape, composition, and organization in aqueous medium is a current challenge. Herein we report construction of supramolecular charge-transfer complex one-dimensional (1D) nanowires consisting of highly ordered mixed-stack π-electron donor–acceptor (D–A) domains. We synthesized n-type and p-type β-sheet forming short peptide-chromophore conjugates, which assemble separately into well-ordered nanofibers in aqueous media. These complementary p-type and n-type nanofibers coassemble *via* hydrogen bonding, charge-transfer complex, and electrostatic interactions to generate highly uniform supramolecular n/p-coassembled 1D nanowires. This molecular design ensures highly ordered arrangement of D–A stacks within n/p-coassembled supramolecular nanowires. The supramolecular n/p-coassembled nanowires were found to be formed by A–D–A unit cells having an association constant (K_A) of 5.18×10^5 M^{-1}. In addition, electrical measurements revealed that supramolecular n/p-coassembled nanowires are approximately 2400 and 10 times more conductive than individual n-type and p-type nanofibers, respectively. This facile strategy allows fabrication of well-defined supramolecular electroactive nanomaterials in aqueous media, which can find a variety of applications in optoelectronics, photovoltaics, organic chromophore arrays, and bioelectronics.

KEYWORDS: *nanowires, self-assembly, coassembly, supramolecular, peptide chromophore, conductivity*

S upramolecular electronics is an emerging research field, which exploits noncovalent interactions to assemble π-conjugated molecular elements into well-defined nanomaterials with semiconductor properties such as light emission, light harvesting, and charge carrier transport for optoelectronic, photovoltaic, bioelectronics, and tissue engineering applica-

Scheme 1. Chemical Structures of (a) p-Type PC (pPC) and (b) n-Type PC (nPC) Molecules and (c) Coassembly of p- and n-Type Nanofibers into Supramolecular n/p-Coassembled Nanowire
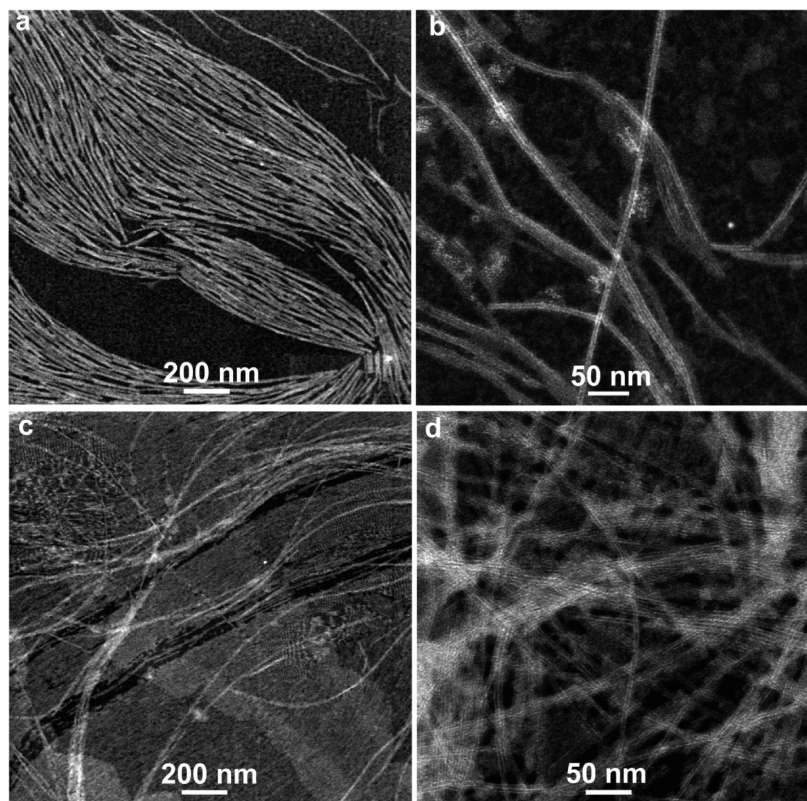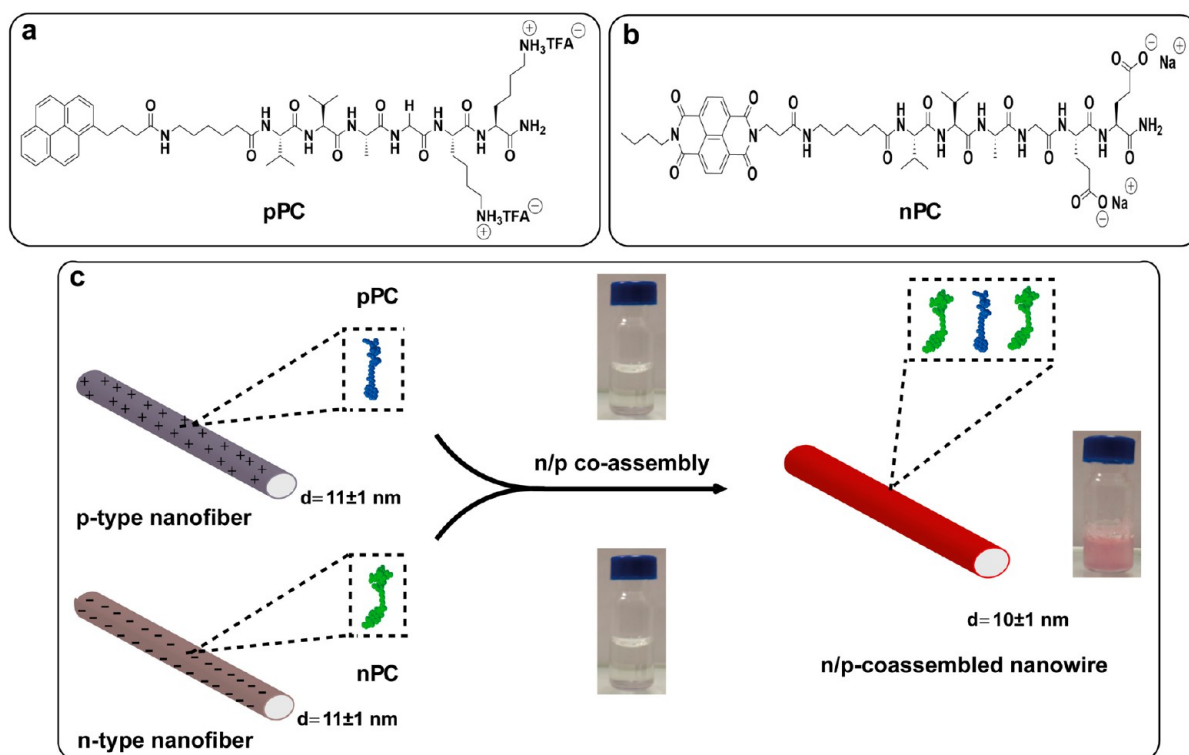

Figure 1. STEM images of pPC (a and b) and nPC (c and d) nanofibers with diameter of 11 ± 1 nm.

tions.[1−4] Efficiency of charge transport, energy migration, and mobility of charge carriers in these supramolecular one-dimensional (1D) nanowires is directly dependent on supra-molecular order of π-conjugated chromophores.[4,5] Therefore, achieving efficient cofacial π−π interactions among hydro-phobic semiconducting chromophores in aqueous medium is a
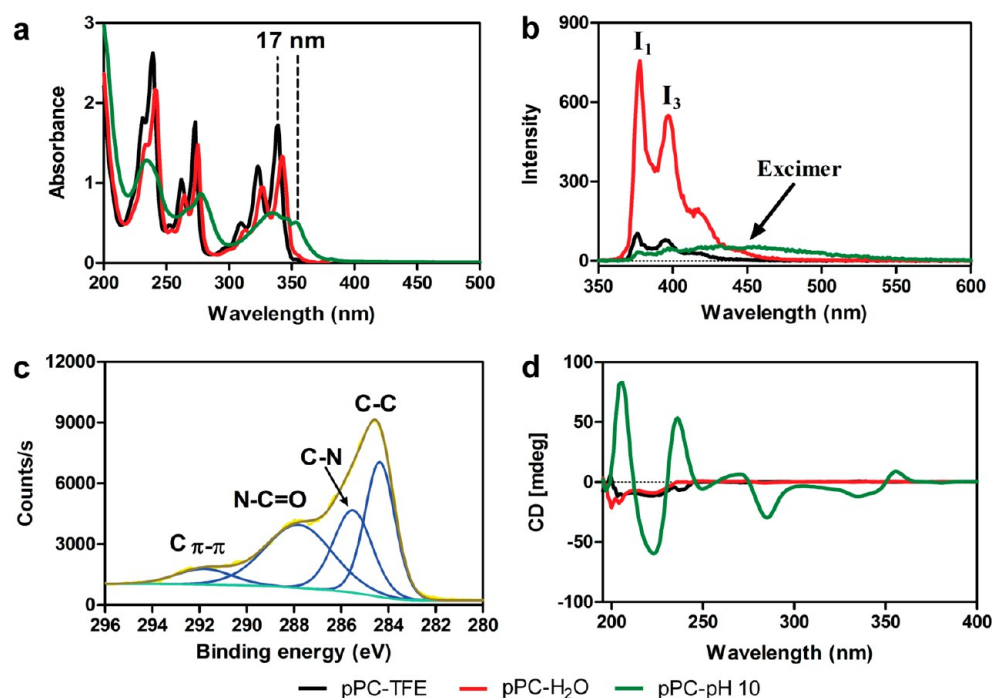
Figure 2. Spectroscopic characterization of pPC assembly. (a) UV−vis absorption and (b) fluorescence emission spectra (excitation wavelength = 340 nm) of pPC. (c) XPS analysis (Gaussian deconvolution of the C 1s signal) of assembled pPC powder and (d) CD spectra of pPC molecules.

highly desired goal in the area of supramolecular electronics. A promising strategy to fabricate 1D electroactive nanomaterials with maximum cofacial π−π interactions in aqueous media is to conjugate n-type or p-type semiconducting molecules to self-assembling short peptide sequences.[2,6] Particularly, conjugation to β-sheet forming peptides not only ensures solubility of hydrophobic semiconducting building blocks in aqueous media but also allows directing long-range spatial organization of semiconducting chromophores.[7,8] The n-type and p-type semiconducting supramolecular nanowires usually suffer from low conductivities.[9−11] To address this problem, p-type and n-type semiconducting 1D nanowires are doped either by an oxidizing (iodine)[11] or reducing agents (hydrazine),[10] respectively. Another strategy is to assemble suitable π-electron donor (D) with an π-electron acceptor (A) in alternating manner to form charge-transfer complexes (CTC) with improved (photo) conductivities.[11−13] Lopez-Andarias *et al.* demonstrated that fabricated CTC made up of alternately segregated D−A nanodomains exhibited tremendous photoconductivity of 0.8 cm² V⁻¹ s⁻¹.[12] Similarly, Nalluri *et al.* constructed CTC xerogels composed of D−A domains enhancing the conductivity up to 10⁶-fold.[11] Despite promising efforts, there are only few reports which illustrate fabrication of well-defined supramolecular n/p-nanowires in aqueous medium.[12,14,15]

Here we report fabrication of well-defined supramolecular n/p-coassembled nanowires in aqueous media. We designed and synthesized β-sheet forming p-type peptide-chromophore (pPC) (Scheme 1a) and n-type peptide-chromophore (nPC) (Scheme 1b) conjugates. Positively charged pPC and negatively charged nPC molecules individually assemble into highly uniform p-type and n-type nanofibers, respectively, with diameter of 11 ± 1 nm and microns in length as imaged by scanning transmission electron microscope (STEM) (Figure 1). These complementary p-type and n-type nanofibers

coassemble *via* hydrogen bonding, CTC, and electrostatic interactions to generate well-ordered supramolecular n/p-coassembled 1D nanowires (Scheme 1c). This smart molecular design ensures highly ordered arrangement of D−A stacks within n/p-coassembled 1D nanowires. Our findings demonstrate that supramolecular n/p-coassembled 1D nanowire is formed from A−D−A unit cells having a strong K_A of 5.18 × 10⁵ M⁻¹. These supramolecular n/p-coassembled nanowires exhibit 2400- and 10-fold enhanced conductivity than the individual n-type and p-type nanofibers, respectively.

RESULTS/DISCUSSION

In this study, pyrene (π-basic with molecular quadrupole moment Qzz = −13.8 B) was conjugated to a β-sheet forming hexapeptide sequence (H₂N-Ahx-VVAGKK-Am)[16] as π-electron donor (D) by using a solid-phase peptide synthesis (SPPS) method to synthesize pPC molecule (Figures S1−3). In this molecular design, VVA residues promote β-sheet formation, and KK residues not only ensure solubility of hydrophobic pyrene molecules in aqueous media but also provide positive charge (Figure S1). A six-carbon linker (Ahx) was introduced between pyrene chromophore and hexapeptide to provide flexibility among chromophores and allow them to arrange favorable orientation during self-assembly process. Aggregation of pPC molecule was studied by UV−vis, fluorescence, circular dichroism (CD), and X-ray photoelectron spectroscopies (XPS). Absorption of pPC molecules in trifluoroethanol (pPC-TFE) and in water (pPC-H₂O) showed well-resolved vibronic structures ranging from 250 to 350 nm, which is characteristic for monomer pyrene chromophores (Figure 2a).[17] A minor red shift in pyrene maxima was observed going from TFE (pPC-TFE) to H₂O (pPC-H₂O), which can be attributed to both solvent polarity difference and partial aggregation of pPC molecules in water. Upon complete charge neutralization by increasing the pH to 10 (pPC-pH 10),
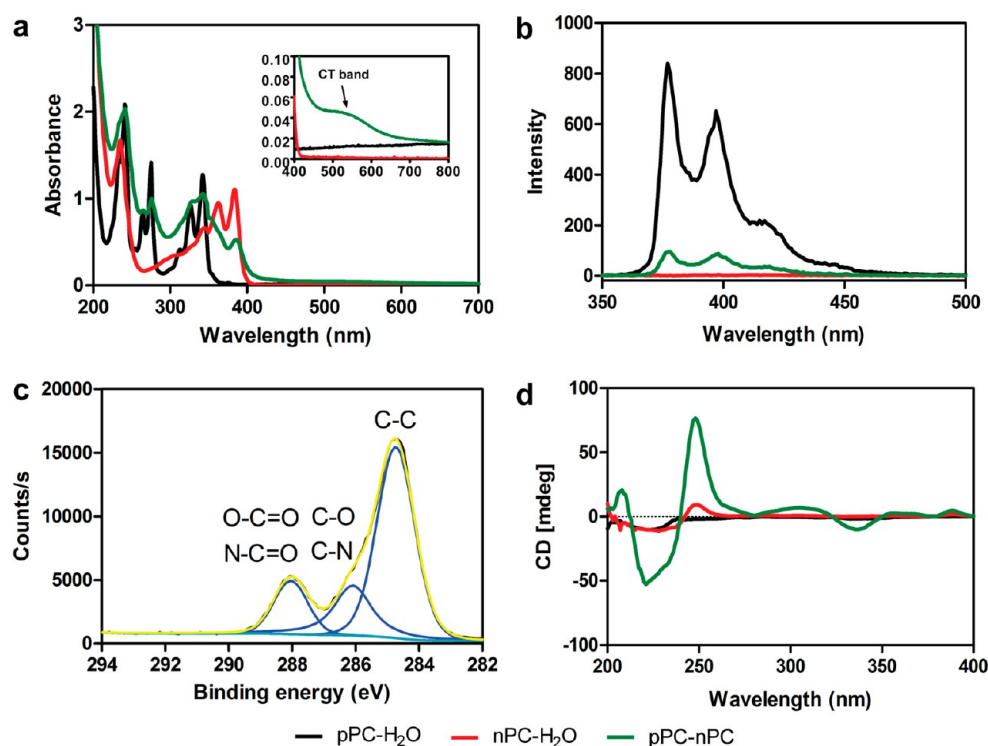
Figure 3. Spectroscopic characterization of pPC and nPC coassembly. (a) UV−vis absorption spectra and inset shows appearance of CT band. (b) Fluorescence emission spectra (excitation wavelength = 340 nm) of pPC-nPC CT complex. (c) XPS analysis (Gaussian deconvolution of the C 1s signal) of pPC-nPC powder and (d) CD spectra of pPC and nPC coassembly in aqueous media.

the pPC molecules demonstrated a 17 nm red-shift followed by a decrease in intensity and broadening of absorption bands. These drastic changes in absorption bands revealed *J*-type $\pi-\pi$ interactions among pyrene molecules within p-type nanofibers.[17] The emission profile of pPC in water (pPC-H$_2$O) showed vibronic structures which is caused by pyrene monomers (Figure 2b). The ratio of emission vibronic peaks I$_3$ (375 nm) and I$_1$ (395 nm) is extremely sensitive to polarity of the solvent and is widely used to probe the vicinity of highly hydrophobic pyrene chromophores.[18] Electrostatic repulsions caused by protonated amine ($-NH_3^+$) groups of lysine residues prevent complete aggregation, thus pyrene molecules are exposed to relatively hydrophilic environment as the value of vibronic peaks (I$_3$/I$_1$) is less than unity (pPC-H$_2$O). Upon charge neutralization by increasing the pH to 10 (pPC-pH 10), a drastic quenching in emission intensity of pPC followed by appearance of a new broad emission (440−550 nm) peak, which corresponds to pyrene excimers (Figure 2b).[18] Planar luminophoric molecules such as perylene and pyrene can experience aggregation-caused quenching (ACQ) at high concentrations.[19] During aggregation of pPC molecules in basic media (pPC-pH 10), local concentration of pyrene molecules within pPC nanofibers increases and experiences strong $\pi-\pi$ stacking interactions, as we observed in XPS spectrum (Figure 2c). Strong $\pi-\pi$ stacking interactions among pyrene moieties cause formation of species like excimers (Figure 2b), hence leading to the observed ACQ effect.

Self-assembly of pPC molecules triggered by charge neutralization does not only allow $\pi-\pi$ stacking of pyrene molecules but also allows them to closely position in a relatively hydrophobic environment (core of p-type nanofibers) as the ratio of vibronic peaks (I$_3$/I$_1$) exceeds unity (Figure 2b). Lyophilized pPC-pH 10 powder analyzed by XPS exhibited a

peak at 292 eV (Figure 2c), which further confirmed the presence of $\pi-\pi$ stacking among closely spaced and spatially constrained pyrene molecules within pPC nanofibers.[20]

To investigate the long-range spatial organization of pyrene molecules within the p-type nanofibers, we further conducted CD analysis (Figure 2d). At basic conditions (pPC-pH 10), the pPC showed a strong bisignate signal with a negative Cotton effect between 200 and 230 nm, which is attributed to formation of β-sheet secondary structures.[21] In addition, weak CD signals were observed between 250 and 360 nm, which confirms induction of chirality to pyrene chromophores via pPC self-assembly. On the other hand, partial aggregation of pPC molecules in water (pPC-H$_2$O) and in TFE (pPC-TFE) did not show significant CD signals (Figure 2d).

Naphthalenediimides (NDIs) are widely studied n-type organic semiconductors with potential applications in organic-field transistor, light harvesting systems, and photovoltaics.[22] NDI (π-acidic with Q$_{zz}$ = +18.6 B) as π-electron acceptor (A) forms preferentially CT complex with π-electron donor pyrene (D). Owing to maximum overlap of LUMO$_{NDI}$ with HOMO$_{pyrene}$, NDI-pyrene CT complex can have large K_A values.[23] Therefore, NDI was functionalized (Figures S4−9) to be compatible with the SPPS method and then was conjugated to a β-sheet forming hexapeptide sequence (H$_2$N-Ahx-VVAGEE-Am) to obtain a nPC molecule bearing negative charge (S10−12). The nPC molecule was designed to have a similar molecular size, sequence, and complementary charge with pPC. The nPC in mild basic condition (nPC-H$_2$O) and in TFE (nPC-TFE) demonstrated two absorption bands at 240 nm and in the range of 300−400 nm, which are due to $\pi-\pi^*$ transitions polarized along the short and long axis of the NDI monomer, respectively (Figure S13a).[24] A small bathochromic shift in NDI maxima (Figure S13a) was observed from TFE
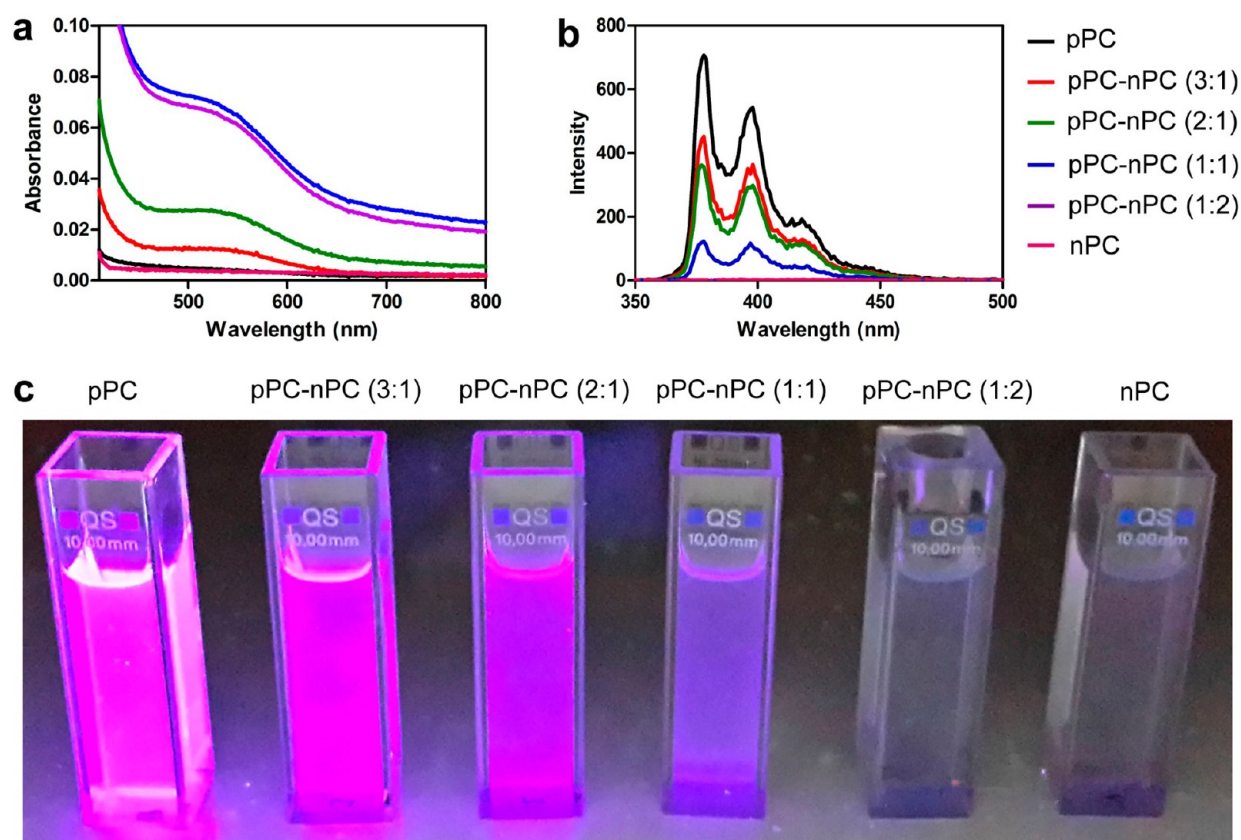
Figure 4. UV−vis absorption of CTC formation (a) and fluorescence quenching measurements (b) of pPC by nPC at different molar ratios. Quenching of pPC by nPC under 254 nm illumination (c).

(nPC-TFE) to H_2O (nPC-H_2O), which can be attributed to both solvent polarity difference and partial aggregation of amphiphilic nPC molecules in mild basic media despite charge repulsions caused by carboxylate groups (COO^-). Decreasing the pH to 2 (nPC-pH 2) caused an 8 nm red-shift, followed by shrinkage in absorption intensity in the range of 300−400 nm. Decrease in the absorption intensity and bathochromic shift in the absorption bands shows the presence of J-type $\pi-\pi$ interactions among NDI chromophores within n-type nanofibers.[24] The nPA solution excited at 340 nm (Figure S13b) did not show any emission, and due to the electron-deficient character of NDI, we observed a very weak signal at 292 eV, which confirms the presence of $\pi-\pi$ stacking among NDI molecules within nPC nanofibers (Figure S13c).

We further investigated long-range organization of NDI chromophores within the supramolecular n-type nanofibers by carrying out CD spectroscopy of nPC in different conditions (Figure S13d). Partially assembled nPC in mild basic condition (nPC-H_2O) and in TFE (nPC-TFE) reveal weak signals in CD (Figure S13d). In contrast, acid triggered assembly of nPC (nPC-pH 2) demonstrated a strong excitonic Cotton effect in the range of 200−230 nm corresponding to highly ordered β-sheet secondary structures. Moreover, chiral signals between 240 and 400 nm were also observed due to $\pi-\pi^*$ transitions polarized along the short and long axis of the NDI monomer, verifying assembly of highly ordered chiral NDI chromophores within nPC nanofibers.[24]

After investigation of individual self-assembly of pPC and nPC peptides in aqueous environment, we studied their coassembly, which formed a new hybrid material by utilizing hydrogen bonding, charge-transfer interactions, and electro-static attractions among positively charged amine groups (NH_3^+) of pPC and negatively charged carboxylate groups (COO^-) of nPC nanofibers. When transparent solutions of pPC (pH ∼ 5) and nPC (pH ∼ 8) were mixed in a 1:1 ratio, a pink color solution was observed (pH ∼ 7), which is an indication of formation of pPC-nPC (n/p-coassembled) CTC (Figure S14a).[23] Similarly, UV−vis spectroscopy analysis of pPC-nPC in aqueous media demonstrated a new broad absorption band at 520 nm, which is attributed to the charge-transfer (CT) band of NDI-pyrene (Figure 3a).[23] Emission of highly fluorescent pPC nanofibers was quenched as soon as nPC nanofibers were mixed, which further confirms effective interaction between pPC and nPC and formation of n/p-coassembled CT complex (Figure 3b). Quenching of fluorescence was not followed by appearance of pyrene excimer emission, which is prevented by successful incorporation of NDI molecules between pyrene chromophores in n/p-coassembled CT complex. The $\pi-\pi$ stacking (292 eV) present in the self-assembled pPC and nPC nanofibers disappeared when the CTC was formed between pPC and nPC moieties (Figure 3c). This further confirms the interaction of pyrene-NDI molecules within n/p-coassembled CTC.

Coassembly of pPC and nPC nanofibers triggered by electrostatic attractions and CTC interactions was further studied by CD spectroscopy (Figure 3d). Individual solutions of pPC and nPC nanofibers revealed flat signals in CD, while their coassembly *via* charge neutralization induced chiral signals. The signals at 220−230 nm confirm the presence of highly ordered β-sheet secondary structures.[21] Moreover, we observed chiral peaks between 220 and 400 nm, which are attributed to pyrene and NDI molecules. CD results revealed
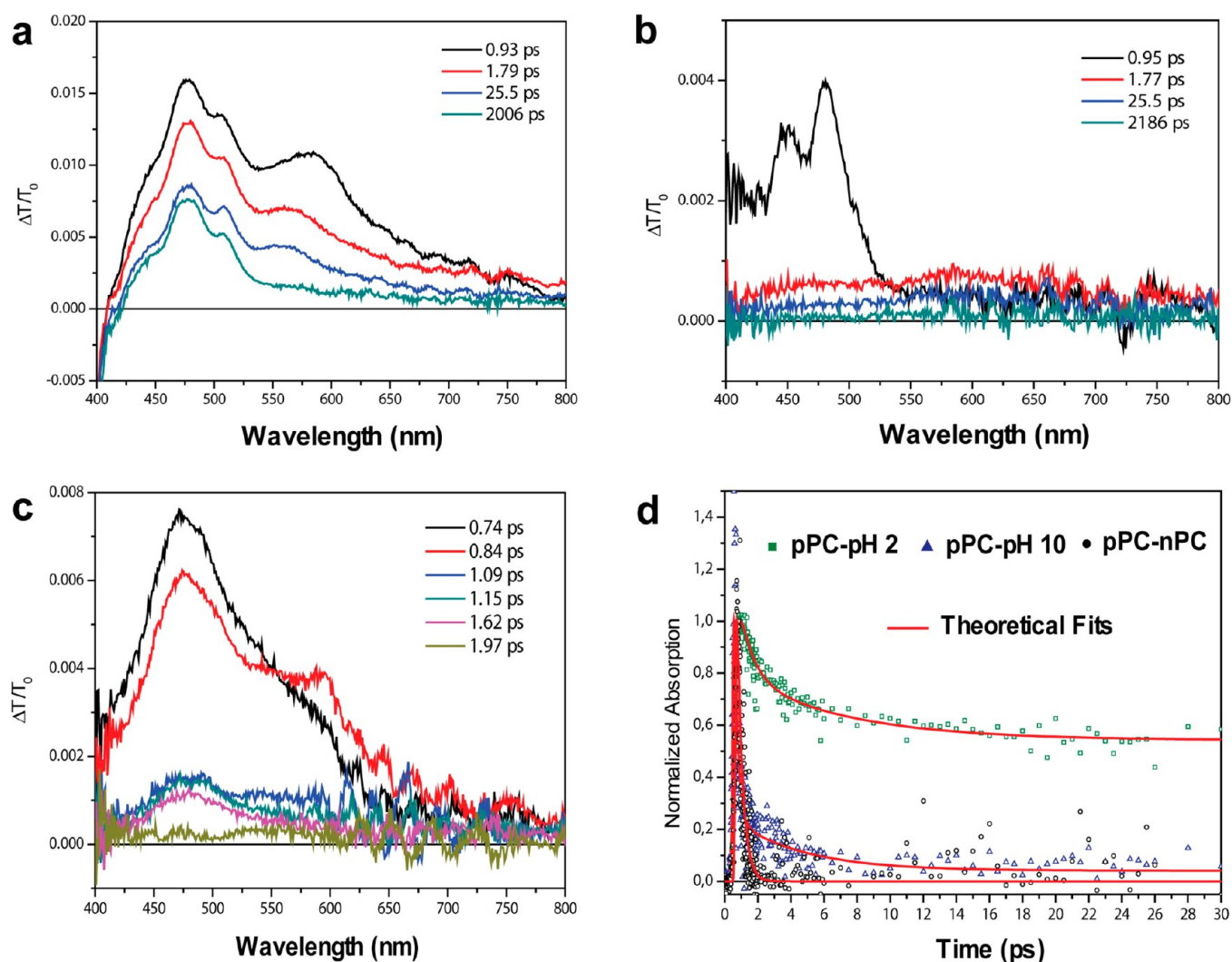
Figure 5. Transient absorption spectra of pPC-pH 2 with different time delays upon excitation at 340 nm (a). Transient absorption spectra of pPC-pH 10 (b) and pPC-nPC (c) with different time delays upon excitation at 350 nm. Decay curves of pPC-pH 2 and pPC-pH 10 samples and pPC-nPC CT complex pair at 477 nm probe wavelength (d).

that coassembly pPC and nPC into n/p-coassembled CTC induces chirality and long-range spatial organization to achiral pyrene and NDI molecules. Furthermore, CD spectroscopy of pPC and nPC coassembly showed that β-sheet signature and chiral signals in pPC-nPC solution are not merely a mathematical sum of individual CD spectra of pPC and nPC components (Figure 3d). This confirms that oppositely charged pPC and nPC nanofibers mix up and form a single aggregate structure.[25]

We further performed titration experiments to assess how pPC and nPC molecules coassemble at different molar ratios. The pPC solutions of fixed concentrations were titrated with nPC solutions, and formation of CTC was monitored by UV–vis and fluorescence spectroscopies (Figure 4). As the molar ratio of the nPC increases in the solution, the CT band at 520 nm increases (Figure 4a), and meanwhile emission of pyrene quenches (Figure 4b) until all pyrene molecules are complexed with NDI. Quenching of pPC by nPC can also be clearly observed with 254 nm illumination (Figure 4c).

Upon self-assembly, intermolecular charge transfer is expected to increase, causing the lifetime of the excited state absorption signals to reduce.[26,27] We performed ultrafast

pump–probe spectroscopy experiments to study the intermolecular charge transfer within n/p-coassembled CT complex (Figure 5). Partially aggregated pPC (pPC-pH 2), self-assembled pPC (pPC-pH 10), and n/p-coassembled (pPC-nPC) samples were investigated. Pump wavelength was chosen based on the linear absorption spectra (340–350 nm), while white light continuum was used as the probe beam for all of the samples. A broad excited-state absorption signal was observed in the white light continuum spectra for all samples (Figure 5a–c), which is caused by aggregation of the samples.

Charge transfer between self-assembled pyrene molecules (pPC-pH 10) or between donor and acceptor chromophores (pPC-nPC) decreases electron population of the excited state, which is pumped. Therefore, not only the magnitude of excited-state absorption signal (S1 → Sn) but also its lifetime are decreased (Figure 5b–c). Since charge transfer is very weak for pPC-pH 2, we observed a strong and broad ESA signal with a very long lifetime (Figure 5a). On the other hand, pPC-pH 10 and pPC-nPC samples have strong charge transfers, and therefore, their relative ESA signals are very small compared to that of pPC-pH 2. In addition, the transient absorption spectra show that the ESA signal of pPC-pH 2 does not completely
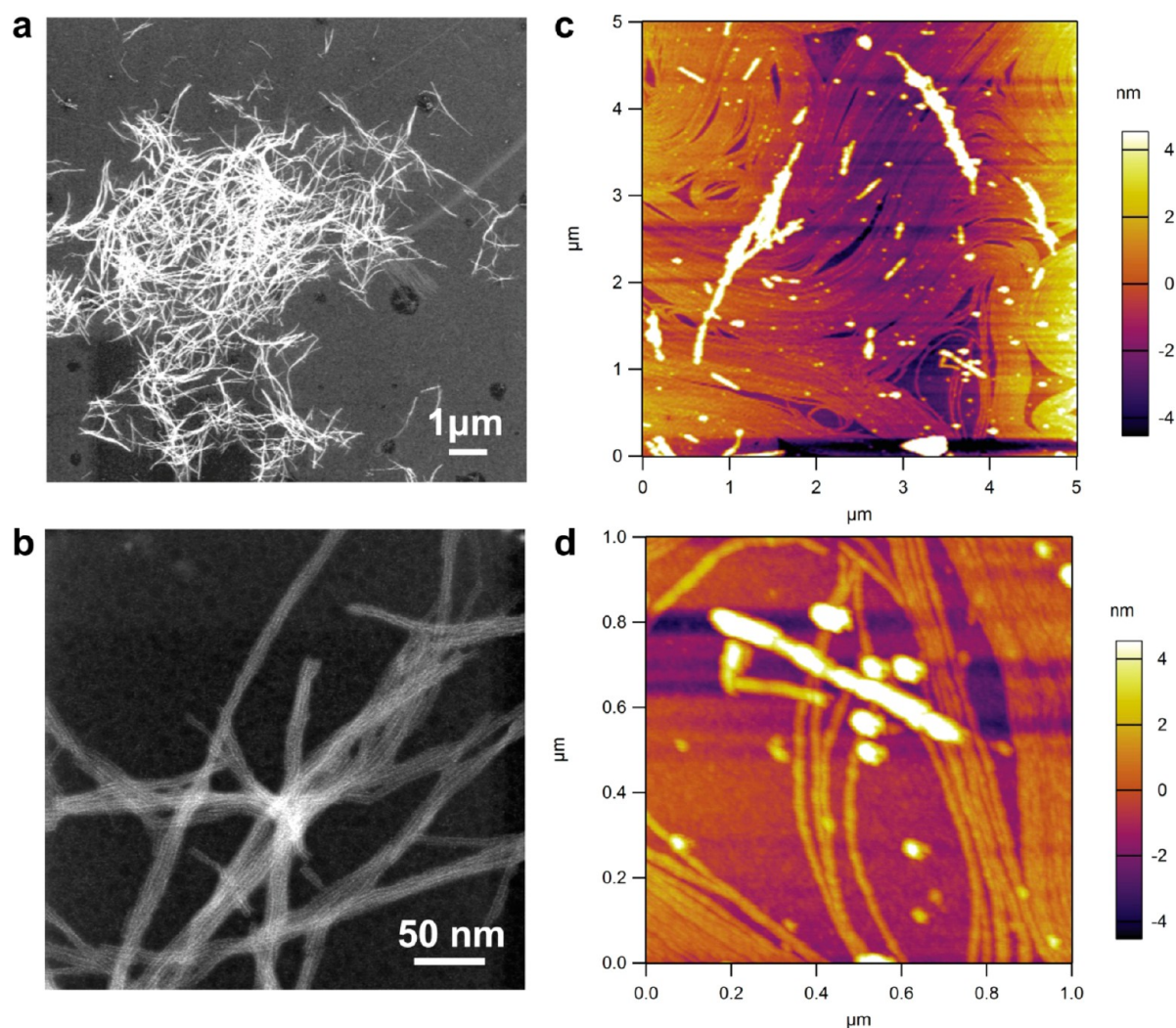
Figure 6. Imaging of n/p-coassembled CTC. STEM images (a and b) and AFM images (c and d) of n/p-coassembled supramolecular nanowires.

decay in 2 ns, while that of pPC-pH 10 and pPC-nPC decays in 100 ps time delay (Figure 5a−c). Figure 5d shows decay curves of normalized excited-state absorption signal at 477 nm probe. Decay time components were measured as 7 ps, 4 ps, and 300 fs for samples pPC-pH 2, pPC-pH 10, and pPC-nPC, respectively. A faster decay of the excited-state absorption signal of pPC-pH 10, than that of pPC-pH 2, is an indication of aggregation at high pH. Furthermore, the fastest decay time component (300 fs) of pPC-nPC CTC within the investigated samples is the indication of stronger charge transfer among pPC and nPC molecules. These results are in good agreement with the fluorescence experiments showing that the coassembly process causes fluorescence quenching of the investigated pPC-nPC CT complex.

STEM images of positively stained supramolecular n/p-coassembled CTC reveal a network of highly uniform nanofibrous morphology with a diameter of 10 ± 1 nm and microns long in length (Figure 6a−b). These results confirmed that the average diameter of n/p-coassembled supramolecular nanowires is similar to those of individual pPC and nPC nanofibers. Moreover, imaging of dried n/p-coassembled nanowires samples by atomic force microscopy (AFM) also exhibited formation of highly uniform nanofibrous morphology with height in nanometers and length in microns (Figure 6c−

d). Self-assembling peptides can form nanostructures due to evaporation of water. We also performed contact-mode AFM imaging in solution to reveal n/p-coassembled nanowires are present in the aqueous media. The AFM images at high (27 μM) and low concentrations (3 μM) of pPC-nPC exhibited highly uniform nanofibrous morphology of n/p-coassembled nanowires in solution (Figure S15). The dried n/p-coassembled samples imaged by STEM and AFM exhibiting uniform nanofibers are similar to the ones observed in the solution.

To investigate in depth molecular interactions between pPC and nPC, XPS, FT-IR, and nuclear Overhauser effect spectroscopy (NOESY) were conducted to study the efficient electrostatic interactions between positively charged amine groups (NH_3^+) of the pPC and negatively charged carboxylate groups (COO^-) of the nPC within n/p-coassembled supramolecular nanowires. The pink suspension of n/p-coassembled nanowires was centrifuged at 8500 rpm, and the upper solution part was decanted, followed by addition of fresh water and centrifuged again. This procedure was repeated several times to get rid of any uncomplexed pPC and nPC molecules and then lyophilized to get a pink powder (Figure S14b). XPS analysis of the pPC powder shows the existence of F 1s at 689 eV (Figure S16a), which corresponds to presence of the counterion

trifluoroacetate anion (TFA⁻).[28] Meanwhile, nPC powder shows Na 1s at 1072 eV (Figure S16b) which is attributed to the presence of counterion sodium cation (Na⁺). On the other hand, no significant signal at 689 eV (F 1s) and 1072 eV (Na 1s) in n/p-coassembled CTC powder (Figure S16c) was observed, which is due to efficient electrostatic interactions between NH_3^+ and COO^- groups where Na⁺ and TFA⁻ form a soluble sodium trifluoroacetate salt, which is washed away during centrifugation steps. FTIR measurements further confirmed the removal of sodium trifluoroacetate during washings, as the C−F stretching mode (1110−1220 cm⁻¹) completely disappeared in n/p-coassembled CTC powder (Figure S16d).[29] To further elucidate the electrostatic interactions within n/p-coassembled nanowires, we carried out 2D NOESY, which is a powerful nuclear magnetic resonance (NMR) technique for structural studies. When a proton is close in space (>5 Å) to another proton (or any other nuclei with spin >0), their magnetic dipoles interact, therefore it can be easily detected by NOESY technique. A typical distance between D−A CTC and β-sheet structure is approximately in the range of 3−5 Å. Hence, interacting protons of the pPC with the nPC are within this range and can easily be detected. We observed close contacts (<3 Å) between Glu-H$_\beta$ protons of nPC and Lys-H$_\varepsilon$ protons of pPC (Figure S17), which further proved that the pPC and the nPC are positioned in close proximity by electrostatic interactions within the supramolecular n/p-coassembled nanowires.[25]

Pyrene and NDI moieties can form a variety of CT complexes in different molecular structures such as A−D, D−A−D, and A−D−A, where each CT complex has specific thermodynamic parameters and K_A values.[30,31] UV−vis, XPS, mass spectrometry (MS), and isothermal titration calorimetry (ITC) were carried out to determine the accurate molecular structure of CT complex and its K_A value. We used the Job's method to estimate the stoichiometry of pPC-nPC.[32] Solutions of the pPC and the nPC were mixed in known ratios to form the CT complex where the total concentrations of the pPC and the nPC in solution were kept constant (Figure S18). Absorbance at 520 nm (CT band) was plotted against the molar ratio of the nPC, and the maximum absorbance value intersecting x-axis corresponds to the stoichiometry of D−A (Figure S18b). The two maxima show the presence of two different CTC including pPC-nPC (1:1) and pPC-nPC (1:2).

Gaussian deconvolution of the N-1s signal can be exploited to determine the populations of electronically distinct N atoms in pPC-nPC CTC.[12] Deconvolution of the total N 1s signal intensity (Figure 7a) reveals 7% of N atoms arising from protonated amines ($R''-NH_3^+$) and 93% of N atoms arising from amide groups ($R'-NHR$) in pPC-nPC CTC. In order to determine the binding ratio of pPC to nPC according deconvolution results, we needed to construct such a CTC with 7% of N atoms that are protonated ($R''-NH_3^+$) and 93% of N atoms that arise from amide groups ($R'-NHR$). Only the CT complex with pPC-nPC (1:2) structure satisfies the deconvolution results (Figure S19). Mass spectrometry of pPC-nPC CT complex shows a signal at 1582 m/z, which further supports that pPC molecules are sandwiched between two nPC molecules (nPC-pPC-nPC) (Figure S20). Results obtained from spectroscopic techniques verify the presence of pPC-nPC (1:2) unit cells within n/p-coassembled nanowires.

ITC was performed to further support the spectroscopic results. A very strong association constant of (K_A) of 5.18×10^5 M⁻¹, enthalpy (ΔH) of −7215 cal/mol and entropy (ΔS) of
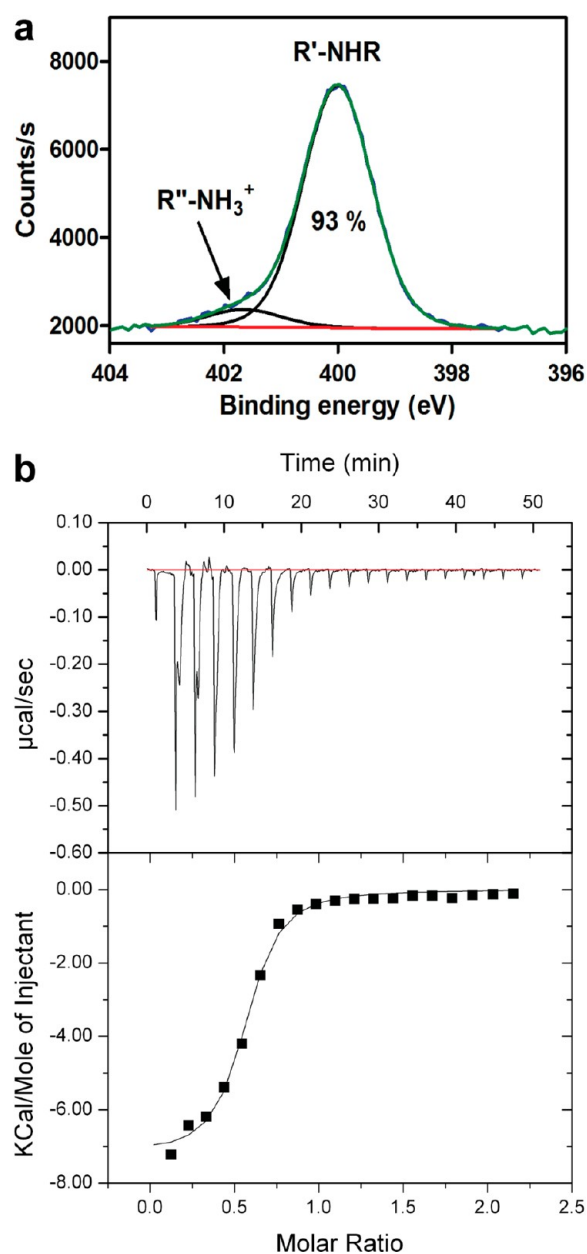

Figure 7. Gaussian deconvolution of the N 1s signal of pPC-nPC CTC acquired by XPS (a). Isothermal calorimetry titration of nPC (0.1 mM) by pPC (1 mM) and binding isotherm of heat of formation against molar ratio of pPC/nPC (b).

1.95 cal/mol deg were calculated from isothermal titrations (Figure 7b). Owing to synergic interactions arising from charge-transfer formation, hydrogen bonding, and electrostatic interactions between the pPC and the nPC molecules, a very strong K_A value was obtained for n/p-coassembled nanowires. A negative Gibbs energy ($-\Delta G$) can easily be calculated from measured ΔH and ΔS values, which confirms highly favorable coassembly of pPC and nPC nanofibers to form n/p-coassembled nanowires in aqueous medium. Moreover, a ratio of 1:2 was also calculated for the pPC: nPC from binding isotherm of heat of formation against molar ratio of pPC/nPC (Figure 7b).

In addition, we further investigated the role of Coulombic attractions and charge-transfer interactions as key driving forces to form n/p-coassembled nanowires. Therefore, we synthesized
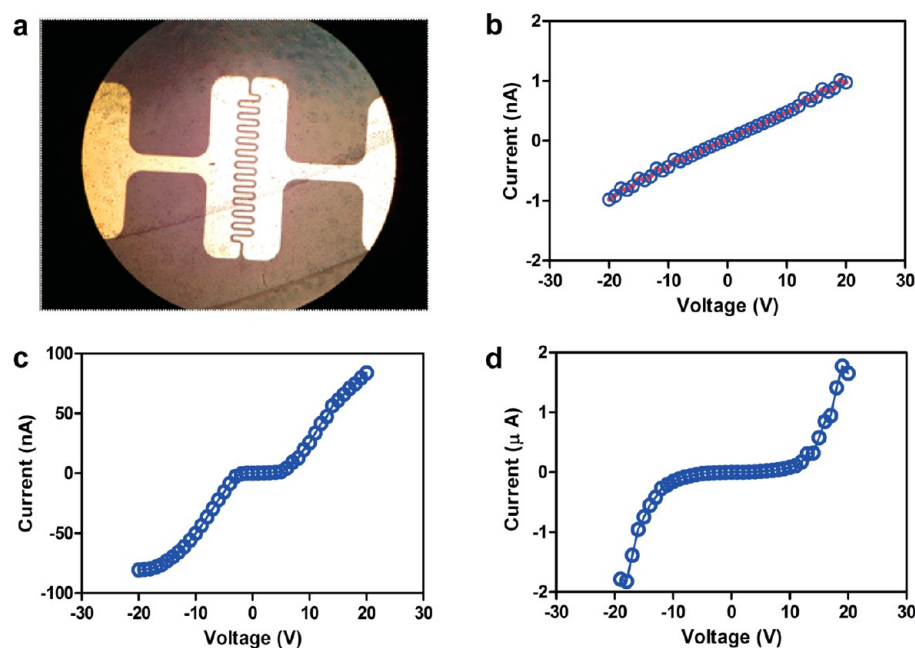
Figure 8. Optical microscope image of a single device after forming Au contacts (a). Current−voltage (*I*−*V*) characteristics of the nPC (b), pPC (c), and the pPC-nPC films (d). Red line is the regression line for the *I*−*V* curve measured for the nPC film.

a new peptide molecule (nPA2), which is analogous to nPC but with positive charge (Figure S21−23). Uranyl acetate stained nPC2 sample was imaged by transmission electron microscope (TEM) showing a diameter of 11 ± 1 nm and microns in length (Figure S24). All peptide molecules (pPC, nPC, and nPC2) showed similar nanofibrous morphology with diameters of 11 ± 1 nm and microns in length. When a solution of pPC is mixed with nPC2 into 1:1 ratio (pPC-nPC2), we observed a pale purple color, which is evidence for the formation of CTC, but the color change is not as intense as in case of pPC-nPC with the same concentration (Figure S25a). In the absence of electrostatic attractions (pPC-nPC2), the CT band shows an absorbance of 0.01 (Figure S25b), while in the presence of Coulombic attractions (pPC-nPC), the CT band jumps to 0.05 absorbance intensity (Figure S25b). This experiment provides valuable information regarding the coassembly process. The supramolecular p-type and n-type nanofibers are highly dynamic in nature, and there is exchange of pPC and nPC2 molecules within the nanofibers to form CTC in the absence of electrostatic interactions. The UV−vis absorption spectra (Figure S25b) clearly showed that we have low concentrations of pPC-nPC2 CTC in addition to high concentrations of uncomplexed pPC and nPC2 molecules. These pPC and nPC2 molecules can further self-assemble randomly into a variety of aggregates.[33] In the presence of Coulombic attractions (pPC-nPC), we observed that there is a 5-fold increase in absorbance of pPC-nPC CTC, which means that a majority of the pPC and nPC molecules participate in the formation of a CTC. The major driving force for the formation of n/p- coassembled nanowires is Coulombic attractions, while charge-transfer interactions contribute slightly.[15] In other words, electrostatic interactions significantly improve the formation of CTC between pyrene and NDI moieties within n/p-coassembled nanowires. The pPC-nPC and pPC-nPC2 have different absorption profiles (Figure S25b) and solution colors (Figure S26), because the coassembly process in both cases produces different CTC. The mass spectrum of pPC-nPC exhibits a

signal at 1582 *m/z*, whereas pPC-nPC2 exhibits a signal at 2072 *m/z* (Figure S25c). These results reveal the formation of pPC-nPC (1:2) CTC in the presence of Coulombic attractions and pPC-nPC2 (1:1) CTC in the absence of Coulombic attractions. We can conclude that Coulombic attractions are primarily responsible for the formation of n/p-coassembled nanowires which mainly consist of highly ordered nPC-pPC-nPC stacks.

Materials forming CT states can show improved conductivity.[13] Therefore, the conductivity of pPC, nPC, and pPC-nPC films was measured at room temperature using a two-probe technique. Peptide nanofiber films were deposited on precleaned glass substrates by drop casting peptide solutions, followed by drying at 37 °C under vacuum for 24 h. The metal contacts were formed by securing the shadow masks with channel lengths of 10 and 20 μm (Figure S27) on top of the samples. Then gold films were deposited in a thermal evaporator system on the areas of the samples that are not protected by the shadow masks (Figure 8a and Figure S28). The electrical resistance of the films between the contacts was measured by sweeping the voltage on one pad from −20 to 20 V and fixing the other pad's voltage at 0 V while measuring the electrical current from each probe. For an ideal resistor, the current−voltage (*I*−*V*) curve is expected to be linear. The resistance can be calculated as the inverse of the slope for the linear regression curve. The *I*−*V* characteristics of the nPC film exhibit such an ideal resistor behavior (Figure 8b).

However, *I*−*V* curves for the pPC (Figure 8c) and the pPC-nPC (Figure 8d) films are nonlinear suggesting a Schottky barrier between the films and the Au contacts.[34] The Schottky barrier limits the electrical conduction for low electric field levels, thus the resistance readings are taken for large electric field/voltage levels (15−20 V) for these samples. Unlike the resistance, the resistivity is an intrinsic property of the material and does not depend on the device geometry. Hence, the film resistivity values are calculated using the measured resistance values and the device dimensions. The resistance can be modeled as $\rho L/Wt$ for any resistor with a uniform cross-

section, where ρ is the resistivity, L is the channel length, W is the channel width, and t is the film thickness which is obtained from AFM images (Figure S29). Table S2 summarizes the values of three devices for each peptide film and compares the final resistivity and conductivity values. The conductivities of nPC and pPC films are 7.6×10^{-9} S/cm and 1.97×10^{-6} S/cm, respectively. Interestingly, pPC-nPC films demonstrate enhanced conductivity of 1.65×10^{-5} S/cm, which is approximately 2400 times more conductive than nPC films and 10 times more than pPC films. The enhancement in conductivity of pPC-nPC films can be attributed to strong intermolecular charge-transfer interactions between pyrene and NDI moieties to form CT states within n/p-coassembled nanowires.[11,13]

CONCLUSIONS

In summary, we presented self-assembling p-type and n-type peptide-chromophore conjugates. Positively charged pPC and negatively charged nPC molecules individually assembled into highly uniform p-type and n-type nanofibers, respectively, with a diameter of 11 ± 1 nm and microns in length. These complementary p-type and n-type nanofibers coassembled via hydrogen bonding, charge-transfer interactions, and electrostatic interactions to generate highly uniform supramolecular n/p- coassembled 1D nanowires. It was shown that Coulombic attractions are primarily responsible for the formation of n/p-coassembled nanowires in aqueous media. We also demonstrated that supramolecular n/p-coassembled nanowires are formed from nPC-pPC-nPC unit cells having a strong K_A of 5.18×10^5 M^{-1}. Moreover, electrical measurements revealed that supramolecular n/p-coassembled nanowires are about 2400 and 10 times more conductive than individual n-type and p-type nanofibers, respectively. This facile strategy allows fabrication of well-defined supramolecular electroactive nanomaterials in aqueous media, which can find a variety of applications in optoelectronics, photovoltaics, and bioelectronics.

METHODS/EXPERIMENTAL

Synthesis of Peptide Molecules. All peptide molecules were synthesized by using solid-phase peptide synthesis (SPPS) method. The syntheses were performed on MBHA rink amide resin and 2 equiv of fluorenylmethyloxycarbonyl (fmoc) protected amino acids, 1.95 equiv of *o*-benzotriazole-*N*,*N*,*N′*,*N′*-tetramethyl-uroniμm-hexafluorophosphate (HBTU), and 3 equiv of *N*,*N*-diisopropylethylamine (DIEA) for 6 h. Fmoc protecting groups were removed by 20% of piperidine in dimethylformamide for 20 min. The peptides were cleaved from the solid resin by a mixture of trifluoroacetic acid:triisopropylsilane:H$_2$O in the ratio of 95:2.5:2.5 for 2 h. The product was collected into a round-bottom flask by washing the resin with DCM. The DCM was evaporated by rotary evaporation, and cold ether was poured to precipitate the peptide. The final product was collected by centrifuging and then lyophilizing for 72 h to get white powder. In the last step of the synthesis, 2 equiv of commercial available 1-pyrenebutyric acid was used, and the coupling was left for 24 h to get pPC. For nPC and nPC2 peptides syntheses, 1.5 equiv of *n*-Bu-NTA-β alanine was used, and the coupling was left for 24 h.

Preparative High-Performance Liquid Chromatography (prep-HPLC). In purification of positively charged peptide molecules, reverse-phase silica column (C18) and 0.1% TFA in water and 0.1% in ACN were used as the mobile phase, while negatively charged peptide molecules were eluted by 0.1% NH$_4$OH in water and 0.1% NH$_4$OH in ACN. A preparative liquid chromatography system (prep-HPLC Agilent 1200 series) integrated with a sample collector was used.

Liquid Chromatography-Mass Spectrometry (LC-MS). After purification of the peptide molecules by prep-HPLC, the purity of the molecules was determined by Agilent Technologies 6530 Accurate-Mass Q-TOF LC-MS. A Zorbax SB-C18 column and 0.1% formic acid in water and 0.1% formic acid in acetonitrile were used as mobile phase for positively charged molecules and 0.1% NH$_4$OH in water and 0.1% NH$_4$OH in ACN were used for negatively charged peptide molecules.

UV–vis Spectroscopy. The peptide solutions were prepared in a 3 mL quartz cell with a 1 cm path length. Stock solution of pPC was prepared by dissolving 2 mg of pPC in 200 μL of water. Three mL of pPC with a concentration of 55 μM was prepared from stock solution. For nPC peptide, 1.6 mg of molecule was dissolved in 140 μL of 1 mM NaOH plus 25 μL of 0.5 M NaOH. Three mL of nPC with a concentration of 55 μM was prepared from stock solution. The dilutions were performed by 1 mM NaOH to keep the pH around 8. The absorbance was recorded on a CaryBio100 instrument.

Fluorescence Spectroscopy. The peptide solutions were prepared in a 3 mL quartz cell with a 1 cm path length. Stock solution of pPC was prepared by dissolving 2 mg of pPC in 200 μL of dd water. Three mL of pPC with a concentration of 55 μM was prepared from stock solution. For nPC peptide, 1.6 mg of molecule was dissolved in 140 μL of 1 mM NaOH plus 25 μL of 0.5 M NaOH. Three mL of nPC with a concentration of 55 μM was prepared from stock solution. The dilutions were performed by 1 mM NaOH solution to keep the pH around 8. The samples were excited at 340 nm, and excitation slit and emission slit widths were adjusted to 1.5 and 5, respectively. The emission intensities were recorded on a Cary Eclipse fluorescence spectrometer instrument.

Circular Dichroism (CD) Spectroscopy. The peptide solutions were prepared in a 3 mL quartz cell with a 1 cm path length. Stock solution of pPC was prepared by dissolving 2 mg of pPC in 200 μL of dd water. Three mL of pPC with a concentration of 55 μM was prepared from stock solution. For nPC peptide, 1.6 mg of molecule was dissolved in 140 μL of 1 mM NaOH plus 25 μL of 0.5 M NaOH. Three mL of nPC with a concentration of 55 μM was prepared from stock solution. The dilutions were performed by 1 mM NaOH to keep the pH around 8. The samples were measured from 500 to 190 nm with 0.1 data pitch, 100 nm/min scanning speed, 1 nm bandwidth, and 4 s D.I.T. An average of two measurements were adjusted, and sensitivity was selected as standard. All measurements were recorded on a Jasco J-815 CD spectrometer.

X-ray Photoelectron Spectroscopy (XPS). Solutions of pPC and nPC were prepared in dd water, then they were mixed into 1:1 mol ratio to form a reddish suspension (Figure S14a). The suspension was centrifuged at 8500 rpm for 10 min, and the upper part was decanted. Then fresh dd water was added followed by centrifugation. This process was performed for seven times to remove any unbound pPC and nPC molecules. The peptide suspension was freeze-dried to obtain reddish powder. This powder was analyzed by Thermo K-alpha monochromatic high-performance X-ray photoelectron spectrometer. The survey analyses were performed at 10 scans.

Coassembly of pPC and nPC (Titrations). Six different solutions were prepared where the mole of the pPC was kept at 1.65×10^{-7} (55 μM, 3 mL) and the mole ratio of nPC was changed. The mole ratios are as follow: pPC:nPC (1:0), (3:1), (2:1), (1:1), (2:1), and (0:1). The CTC formation was monitored by UV–vis and fluorescence spectroscopy. The samples were excited at 340 nm, and excitation slit and emission slit widths were adjusted to 1.5 and 5, respectively. The pH of the final solution for pPC-nPC is always around 7.

Ultrafast Pump–Probe Spectroscopy. The ultrafast wavelength-dependent pump probe spectroscopy measurements were performed using a Ti:Sapphire laser amplifier-optical parametric amplifier system (Spectra Physics, Spitfire Pro XP, TOPAS) with commercial pump probe setup (Spectra Physics, Helios). Pulse duration was measured as 100 fs with a cross correlation. Wavelengths of the pump beam were 340 nm for pPC molecules and 350 nm for pPC-nPC CT complex. White light continuum was used as a probe beam.

Scanning Transmission Electron Microscopy (STEM). FEI Tecnai G2 F30 transmission electron microscope (TEM) was used to image the stained (2% uranyl acetate solution) peptide nanofibers. Ten μL of peptide solutions prepared for UV−vis and fluorescence spectroscopies were dropped on a carbon-covered copper grid followed by air drying at temperature. The stainings were performed for 90 s.

Atomic Force Microscopy (AFM). Solutions of pPC and nPC were prepared in dd water, then they were mixed into 1:1 mol ratio to form a reddish suspension. The suspension was diluted 100 times, and 10 μL of was dropped on clean silicon wafer. The dried sample was imaged by noncontact mode using a MFP3D Asylum microscope. For imaging of pPA-nPA samples in solution, stock solutions of pPA (55 μL) and nPA (55 μL) were prepared. After mixing and vortexing, 300 μL of the sample was added onto freshly cleaved mica and imaged in aqueous environment with contact mode. Silicon nitride soft contact mode AFM probes (SiNi) from Budget Sensors were used for the imaging.

Fourier Transform Infrared (FT-IR) Spectroscopy. Samples prepared for XPS analyses were pressed into KBr pellets. Only the KBr pellet was used as background. The measurements were recorded on Fourier transform infrared spectrometer (Bruker VERTEX 70). 64 scans were recorded between 4000 and 400 cm^{-1} at a resolution of 4 cm^{-1}.

Nuclear Overhauser Effect Spectroscopy (NOESY). Six mg of pPC was dissolved in D$_2$O, and 6 mg of nPC was dissolved in 500 μL of D$_2$O + 150 μL of NaOD (30% solution). The pPC and nPC solutions were mixed, and NOESY spectrum was recorded at 64 scans using 400 MHz NMR.

Isothermal Titration Calorimetry (ITC). 0.1 mM of nPC (280 μL) solution was titrated by 1 mM of pPC (40 μL) solution using iTC200 system (MicroCal, GE Healthcare). The titration was performed at 25 °C with 400 rpm stirring speed. Reference power was set as 5 μCal/s. Twenty injections were done, where the injection period was 4 s and the space between injections was 150 s. ITC binding isotherms were best fitted by a one-sets of site mode.

Electrical Measurements. Shadow masks from the Ossila Inc. are used with channel lengths of 10 and 20 μm and widths on the order of approximately mm. Prior to forming the metal contacts, the peptide films are deposited on 1.5 × 2 cm^2 precleaned glass substrates. The metal contacts are formed by securing the shadow masks on top of the samples. Then gold films are deposited in a thermal evaporator system on the areas of the samples that are not protected by the shadow masks. The gold evaporation is performed at a pressure of 5 × 10^{-6} Torr. The evaporation rate is 1−2 Å/s, and the final gold thickness is ~50 nm. Electrical measurements were performed using a Keithley parameter analyzer with a microprobe station. Tungsten needles attached to microcontrollers were placed on the large contact pads. The sum of the contact resistance that is the resistance between the tungsten probes and the Au pads and the resistance of the gold extensions are negligibly small (<100 Ω) compared to the lowest resistance values expected from the films (~MΩ).

ASSOCIATED CONTENT

🅢 Supporting Information

The Supporting Information is available free of charge on the ACS Publications website at DOI: 10.1021/acsnano.7b02025.

Experimental details and supplementary figures and methods (PDF)

AUTHOR INFORMATION

Corresponding Author
*E-mail: mguler@uchicago.edu.

ORCID 🅞
Mustafa O. Guler: 0000-0003-1168-202X

Notes
The authors declare no competing financial interest.

REFERENCES

(1) Hoeben, F. J. M.; Jonkheijm, P.; Meijer, E. W.; Schenning, A. P. H. J. About Supramolecular Assemblies of Pi-Conjugated Systems. *Chem. Rev.* **2005**, *105*, 1491−1546.

(2) Tovar, J. D. Supramolecular Construction of Optoelectronic Biomaterials. *Acc. Chem. Res.* **2013**, *46*, 1527−1537.

(3) Hasegawa, M.; Iyoda, M. Conducting Supramolecular Nanofibers and Nanorods. *Chem. Soc. Rev.* **2010**, *39*, 2420−2427.

(4) Channon, K. J.; Devlin, G. L.; MacPhee, C. E. Efficient Energy Transfer within Self-Assembling Peptide Fibers: A Route to Light-Harvesting Nanomaterials. *J. Am. Chem. Soc.* **2009**, *131*, 12520−12521.

(5) Moulin, E.; Cid, J. J.; Giuseppone, N. Advances in Supramolecular Electronics - From Randomly Self-Assembled Nanostructures to Addressable Self-Organized Interconnects. *Adv. Mater.* **2013**, *25*, 477−487.

(6) Ardona, H. A.; Tovar, J. D. Peptide Pi-Electron Conjugates: Organic Electronics for Biology. *Bioconjugate Chem.* **2015**, *26*, 2290−2302.

(7) Eakins, G. L.; Pandey, R.; Wojciechowski, J. P.; Zheng, H. Y.; Webb, J. E. A.; Valery, C.; Thordarson, P.; Plank, N. O. V.; Gerrard, J. A.; Hodgkiss, J. M. Functional Organic Semiconductors Assembled *via* Natural Aggregating Peptides. *Adv. Funct. Mater.* **2015**, *25*, 5640−5649.

(8) Shao, H.; Nguyen, T.; Romano, N. C.; Modarelli, D. A.; Parquette, J. R. Self-Assembly of 1-D n-type Nanostructures Based on Naphthalene Diimide-Appended Dipeptides. *J. Am. Chem. Soc.* **2009**, *131*, 16374−16376.

(9) Amit, M.; Cheng, G.; Hamley, I. W.; Ashkenasy, N. Conductance of Amyloid Beta Based Peptide Filaments: Structure-Function Relations. *Soft Matter* **2012**, *8*, 8690−8696.

(10) Che, Y. K.; Datar, A.; Balakrishnan, K.; Zang, L. Ultralong Nanobelts Self-Assembled From an Asymmetric Perylene Tetracarboxylic Diimide. *J. Am. Chem. Soc.* **2007**, *129*, 7234−7235.

(11) Nalluri, S. K.; Shivarova, N.; Kanibolotsky, A. L.; Zelzer, M.; Gupta, S.; Frederix, P. W.; Skabara, P. J.; Gleskova, H.; Ulijn, R. V. Conducting Nanofibers and Organogels Derived From the Self-Assembly of Tetrathiafulvalene-Appended Dipeptides. *Langmuir* **2014**, *30*, 12429−12437.

(12) Lopez-Andarias, J.; Rodriguez, M. J.; Atienza, C.; Lopez, J. L.; Mikie, T.; Casado, S.; Seki, S.; Carrascosa, J. L.; Martin, N. Highly Ordered *n/p* Co-Assembled Materials with Remarkable Charge Mobilities. *J. Am. Chem. Soc.* **2015**, *137*, 893−897.

(13) Kitamura, T.; Nakaso, S.; Mizoshita, N.; Tochigi, Y.; Shimomura, T.; Moriyama, M.; Ito, K.; Kato, T. Electroactive Supramolecular Self-Assembled Fibers Comprised of Doped Tetrathiafulvalene-Based Gelators. *J. Am. Chem. Soc.* **2005**, *127*, 14769−14775.

(14) Nalluri, S. K. M.; Berdugo, C.; Javid, N.; Frederix, P. W. J. M.; Ulijn, R. V. Biocatalytic Self-Assembly of Supramolecular Charge-Transfer Nanostructures Based on n-Type Semiconductor-Appended Peptides. *Angew. Chem., Int. Ed.* **2014**, *53*, 5882−5887.

(15) Wang, C.; Guo, Y. S.; Wang, Y. P.; Xu, H. P.; Wang, R. J.; Zhang, X. Supramolecular Amphiphiles Based on a Water-Soluble Charge-Transfer Complex: Fabrication of Ultralong Nanofibers with Tunable Straightness. *Angew. Chem., Int. Ed.* **2009**, *48*, 8962−8965.

(16) Khalily, M. A.; Goktas, M.; Guler, M. O. Tuning Viscoelastic Properties of Supramolecular Peptide Gels *via* Dynamic Covalent Crosslinking. *Org. Biomol. Chem.* **2015**, *13*, 1983−1987.

(17) Choi, I.; Park, I. S.; Ryu, J. H.; Lee, M. Control of Peptide Assembly Through Directional Interactions. *Chem. Commun.* **2012**, *48*, 8481−8483.

(18) Garifullin, R.; Guler, M. O. Supramolecular Chirality in Self-Assembled Peptide Amphiphile Nanostructures. *Chem. Commun.* **2015**, *51*, 12470−12473.

(19) Hong, Y. N.; Lam, J. W. Y.; Tang, B. Z. Aggregation-Induced Emission. *Chem. Soc. Rev.* **2011**, *40*, 5361−5388.

(20) Demirel, G. B.; Daglar, B.; Bayindir, M. Extremely Fast and Highly Selective Detection of Nitroaromatic Explosive Vapours Using Fluorescent Polymer Thin Films. *Chem. Commun.* **2013**, *49*, 6140−6142.

(21) Khalily, M. A.; Gulseren, G.; Tekinay, A. B.; Guler, M. O. Biocompatible Supramolecular Catalytic One-Dimensional Nanofibers for Efficient Labeling of Live Cells. *Bioconjugate Chem.* **2015**, *26*, 2371−2375.

(22) Al Kobaisi, M.; Bhosale, S. V.; Latham, K.; Raynor, A. M.; Bhosale, S. V. Functional Naphthalene Diimides: Synthesis, Properties, and Applications. *Chem. Rev.* **2016**, *116*, 11685−11796.

(23) Kumar, N. S. S.; Gujrati, M. D.; Wilson, J. N. Evidence of Preferential Pi-Stacking: A Study of Intermolecular and Intramolecular Charge Transfer Complexes. *Chem. Commun.* **2010**, *46*, 5464−5466.

(24) Shao, H.; Seifert, J.; Romano, N. C.; Gao, M.; Helmus, J. J.; Jaroniec, C. P.; Modarelli, D. A.; Parquette, J. R. Amphiphilic Self-Assembly of an n-Type Nanotube. *Angew. Chem., Int. Ed.* **2010**, *49*, 7688−7691.

(25) Behanna, H. A.; Donners, J. J. J. M.; Gordon, A. C.; Stupp, S. I. Coassembly of Amphiphiles with Opposite Peptide Polarities into Nanofibers. *J. Am. Chem. Soc.* **2005**, *127*, 1193−1200.

(26) Garifullin, R.; Erkal, T. S.; Tekin, S.; Ortac, B.; Gurek, A. G.; Ahsen, V.; Yaglioglu, H. G.; Elmali, A.; Guler, M. O. Encapsulation of a Zinc Phthalocyanine Derivative in Self-Assembled Peptide Nanofibers. *J. Mater. Chem.* **2012**, *22*, 2553−2559.

(27) Nowak-Krol, A.; Fimmel, B.; Son, M.; Kim, D.; Wurthner, F. Photoinduced Electron Transfer (PET) *versus* Excimer Formation in Supramolecular *p/n* heterojunctions of Perylene Bisimide Dyes and Implications for Organic Photovoltaics. *Faraday Discuss.* **2015**, *185*, 507−527.

(28) Stevens, J. S.; de Luca, A. C.; Pelendritis, M.; Terenghi, G.; Downes, S.; Schroeder, S. L. M. Quantitative Analysis of Complex Amino Acids and RGD Peptides by X-Ray Photoelectron Spectroscopy (XPS). *Surf. Interface Anal.* **2013**, *45*, 1238−1246.

(29) Roux, S.; Zekri, E.; Rousseau, B.; Paternostre, M.; Cintrat, J. C.; Fay, N. Elimination and Exchange of Trifluoroacetate Counter-Ion From Cationic Peptides: A Critical Evaluation of Different Approaches. *J. Pept. Sci.* **2008**, *14*, 354−359.

(30) Das, A.; Ghosh, S. Supramolecular Assemblies by Charge-Transfer Interactions Between Donor and Acceptor Chromophores. *Angew. Chem., Int. Ed.* **2014**, *53*, 2038−2054.

(31) Kumar, M.; Rao, K. V.; George, S. J. Supramolecular Charge Transfer Nanostructures. *Phys. Chem. Chem. Phys.* **2014**, *16*, 1300−1313.

(32) Renny, J. S.; Tomasevich, L. L.; Tallmadge, E. H.; Collum, D. B. Method of Continuous Variations: Applications of Job Plots to the Study of Molecular Associations in Organometallic Chemistry. *Angew. Chem., Int. Ed.* **2013**, *52*, 11998−12013.

(33) Draper, E. R.; Lee, J. R.; Wallace, M.; Jackel, F.; Cowan, A. J.; Adams, D. J. Self-Sorted Photoconductive Xerogels. *Chem. Sci.* **2016**, *7*, 6499−6505.

(34) Schroder, D. K.: *Semiconductor Material and Device Characterization*, 3rd ed.; John Wiley & Sons, Inc.: Hoboken, N.J., 2006; pp 157−160.